2,2′:6′,2″-Terpyridine (terpy) acting as a Fluxional Bidentate Ligand. Part 1. Trimethylplatinum(IV) Halide Complexes [PtXMe$_3$(terpy)] (X = Cl, Br or I): Nuclear Magnetic Resonance Studies of their Solution Dynamics and Crystal Structure of [PtIMe$_3$(terpy)]†

Edward W. Abel,[a] Valentin S. Dimitrov,[b] Nicholas J. Long,[a] Keith G. Orrell,*[,a] Anthony G. Osborne,[a] Vladimir Šik,[a] Michael B. Hursthouse[c] and Mohammed A. Mazid[c]

[a] *Department of Chemistry, The University, Exeter EX4 4QD, UK*

[b] *Institute of Organic Chemistry, Bulgarian Academy of Sciences, Sofia 1113, Bulgaria*

[c] *School of Chemistry and Applied Chemistry, University of Wales College of Cardiff, Cardiff CF1 3TB, UK*

2,2′:6′,2″-Terpyridine (terpy) reacts with trimethylplatinum halides [(PtXMe$_3$)$_4$] (X = Cl, Br or I) to form stable octahedral complexes *fac*-[PtXMe$_3$(terpy)] (X = Cl, Br or I) in which the terpy molecule is acting as a bidentate chelate ligand. In solution the complexes are fluxional with the ligand oscillating between equivalent bidentate bonding modes by a mechanism consisting of 'tick-tock' twists of the metal moiety through an angle equal to the N–Pt–N angle of the octahedral centre. At below-ambient temperatures rotation of the unco-ordinated pyridine ring is severely restricted with the most favoured rotamers having the plane of the pendant pyridine ring at an angle of *ca.* 52° with respect to the adjacent co-ordinated pyridine ring plane. The X-ray crystal structure of [PtIMe$_3$(terpy)] depicts the pendant pyridine N atom *cis* to iodine and this is the predominant species in solution at low temperatures. At above-ambient temperatures the complexes exhibit intramolecular Pt–Me exchange of axial and equatorial environments. Energy data based on accurate dynamic NMR fittings are reported for the three dynamic processes, namely pendant pyridine rotation, 1,4-Pt–N metallotopic shifts and Pt–Me scramblings.

Aromatic nitrogen heterocycles are an important class of ligand in co-ordination chemistry. A typical member of the class, 2,2′:6′,2″-terpyridine (terpy) readily forms stable complexes with transition metals and has been extensively used for preparative purposes.[1] Recently, heteroaromatic analogues of terpy, *e.g.* 6-(2-thienyl)-2,2′-bipyridine,[2] and higher oligopyridines, *e.g.* 2,2′:6′,2″:6″,2‴-quaterpyridine[3] have also been investigated as ligands.

2,2′:6′,2″-Terpyridine can in principle exhibit a variety of bonding modes to metals, *viz.* monodentate, bidentate, terdentate and bridging. In practice, however, it almost invariably functions as a terdentate ligand, and although there have been reports[4–7] of compounds in which bidentate bonding is suggested, X-ray crystallographic evidence has been obtained in only three instances,[8–10] involving compounds of ruthenium or rhenium.

We have recently reported[11] preliminary results of a detailed NMR study of some complexes of Pt^{IV}, Re^{I} and W^{0} with terpyridine in which it was demonstrated conclusively that, in solution, the terpy ligand was acting in a bidentate chelate bonding mode, and also undergoing an oscillatory fluxional motion. This paper reports synthetic details of the complexes formed between terpy and trimethylplatinum halides [(PtXMe$_3$)$_4$] (X = Cl, Br or I), extensive NMR studies of three distinct dynamic processes exhibited by these complexes in solution, and the crystal structure of the complex [PtIMe$_3$(terpy)].

Experimental

Materials.—All preparations were carried out using standard Schlenk techniques.[12] All reactions were performed under purified nitrogen using freshly distilled, dried and degassed solvents.

† *Supplementary data available:* see Instructions for Authors, *J. Chem. Soc., Dalton Trans.*, 1993, Issue 1, pp. xxiii–xxviii.

The compounds [(PtXMe$_3$)$_4$] (X = Cl, Br or I) were prepared by published methods.[13–16] 2,2′:6′,2″-Terpyridine (terpy) was purchased from Aldrich Chemical Co. Elemental analyses were performed by Butterworth Laboratories Ltd., Teddington, Middlesex, London.

The three complexes were prepared in a similar fashion. A typical example is outlined below, and details of all synthetic and analytical data are summarised in Table 1.

The complex [(PtClMe$_3$)$_4$] (0.1 g, 0.36 mmol, based on the monomeric unit) was dissolved in benzene (40 cm^3). The solution was filtered and added to a benzene solution (20 cm^3) of terpy (0.085 g, 0.36 mmol). The pale yellow solution was stirred and warmed to 50 °C for 5 h, during which time it became more yellow in colouration. The solution was filtered and then evaporated to dryness under reduced pressure. The resulting solid was washed with hexane (2 × 30 cm^3) and then with benzene (2 × 3 cm^3) to leave a pale yellow solid. The solid was recrystallised from hexane–dichloromethane (1:1) to give pale yellow crystals of *fac*-[PtClMe$_3$(terpy)]. Yield, 0.13 g (71%).

NMR Spectra.—Hydrogen-1 spectra were recorded on a Bruker AM 250 FT spectrometer operating at 250.13 MHz. All chemical shifts are quoted relative to $SiMe_4$ as an internal standard. A BVT-1000 unit was used to control the magnet probe temperature, calibration of which was checked against a Comark digital thermometer. Quoted spectral temperatures are accurate to at least ±1 °C. The ^{195}Pt spectrum of [PtIMe$_3$(terpy)] was recorded on a $CDCl_3$ solution of the complex using a Bruker ACF-300 spectrometer operating at 64.23 MHz for ^{195}Pt. The ^{195}Pt shift is quoted relative to Ξ(^{195}Pt) = 21.4 MHz.

Rate data were based on band-shape analysis of ^{1}H spectra using the authors' version of the standard DNMR program.[17] Matchings of experimental and calculated spectra allowed for temperature dependences of all lineshape parameters, namely rate constants, chemical shift differences and spin–spin relax-

Table 1 Synthetic, melting temperature and analytical data for the complexes [$PtXMe_3$(terpy)] (X = Cl, Br or I)

Complex	Yield[a] (%)	M.p./°C	Analysis[b] (%) C	H	N
1 [$PtClMe_3$(terpy)]	71	190–200 (decomp.)	43.2 (42.5)	4.0 (4.0)	8.2 (8.3)
2 [$PtBrMe_3$(terpy)]	74	203–205 (decomp.)	39.6 (39.1)	3.7 (3.6)	7.6 (7.6)
3 [$PtIMe_3$(terpy)]	81	200–205	34.6 (34.6)[c]	3.3 (3.3)[c]	6.5 (6.4)[c]

[a] Yield quoted relative to the $PtXMe_3$ monomeric unit, reaction time 5 h. [b] Required values given in parentheses. [c] Figures allow for inclusion of solvent of crystallisation (see X-ray structure) *i.e.* [$PtIMe_3$(terpy)]·0.5CH_2Cl_2.

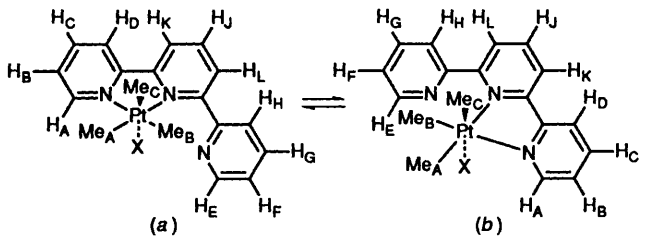

Fig. 1 Interconverting structures of [$PtXMe_3$(terpy)] complexes showing the hydrogen labelling

ation times, as described in the double fitting procedure.[18,19] Activation parameters based on experimental rate data were calculated using the THERMO program.[20] Quoted errors are statistical errors based on scattering of the rate constants around the Eyring straight line only. The $\Delta G^{\ddagger}$ values are also quoted with errors for uncertainties in both rate constants and temperatures.

X-Ray Crystallography.—Crystals of [$PtIMe_3$(terpy)] were prepared as described above and sealed under nitrogen in Lindemann capillaries.

Crystal data. The light orange crystals contained dichloromethane, with a formula [$C_{18}H_{20}IN_3Pt·CH_2Cl_2$], M = 685.29, triclinic, space group $P\bar{1}$, a = 9.398(3), b = 10.377(1), c = 11.692(2) Å, α = 83.52(1), β = 75.93(1), γ = 83.83(2)°, U = 1095.17 Å^3, Z = 2, D_c = 2.08 g cm^{-3}, $F(000)$ = 644, radiation Mo-Kα, λ = 0.710 69 Å, μ = 81.22 cm^{-1}.

Data collection and processing. Data were collected using a FAST TV area detector diffractometer situated at the window of a rotating anode generator operating at 50 kV, 55 mA with a molybdenum anode, as described previously.[21] Somewhat more than one hemisphere of data were recorded for which 7459 reflections were measured, giving 4944 unique and 3880 observed with $F_o > 3\sigma(F_o)$.

Structure analysis and refinement. The structure was solved by standard Patterson methods. Full-matrix least-squares refinement was performed with non-hydrogen atoms assigned anisotropic thermal parameters. Hydrogen atoms were allowed to ride on their parent carbon atoms in the calculated positions (C–H 0.96 Å) and freely refined with group U_{iso} values. The number of parameters in the least squares scheme was 251, with the weighting scheme $w = 1/\sigma^2|F_o|$. The final R, R' values were 0.038, 0.047 respectively. Computer programs used are given in ref. 22.

Additional material available from the Cambridge Crystallographic Data centre comprises H-atom coordinates, thermal parameters and remaining bond lengths and angles.

Results and Discussion

Ambient and Above-ambient Temperature NMR Studies.—Elemental analysis data (Table 1) imply that if six-co-ordinate octahedral platinum(IV) complexes are formed the terpy molecule will be acting as a bidentate chelating ligand [Fig. 1(*a*)]. However, the ill resolved nature of most of the signals in the room-temperature ^{1}H NMR spectra of these complexes (*e.g.* Fig. 2) was immediately suggestive of some form of dynamic co-ordinative bonding for terpy. On cooling solutions of the complexes to *ca.* −20 °C, most of the lines sharpened appreciably and well resolved spectra were obtained. The ^{1}H spectra of the complex [$PtIMe_3$(terpy)] in Fig. 2 will serve as a typical example. Careful analysis of this spectrum with proton decoupling experiments and consideration of the relative shielding/deshielding effects of adjacent pyridine rings established the assignment of all eleven hydrogen nuclei (labelled A–L, Fig. 1) thus confirming a bidentate terpy complex. All aromatic hydrogen chemical shifts are given in Table 2. Most signals show multiplet splittings due to three-bond and also in some cases four-bond couplings to neighbouring hydrogens on the same pyridine ring. No adjacent-ring hydrogen couplings were detected. The signal due to H_H is anomalously broad (see later) so that no multiplet splitting was observed. Signals due to hydrogens H_A and H_E in α positions to heterocyclic N atoms occur at highest frequencies with H_A exhibiting an additional high-frequency co-ordination shift. The H_A signal also exhibits more significant N quadrupole broadening than H_E, and also shows partially resolved ^{195}Pt satellites due to ^3J(Pt–H) scalar coupling.

On warming the $CDCl_2CDCl_2$ solution of the complex, dramatic changes occur in the ^{1}H NMR spectrum as shown in Fig. 2. Exchange occurs between the labelled pairs of signals A/E, B/F, C/G and D/H according to the dynamic spin system ABCD ⇌ EFGH. Exchange also occurs between the signals due to hydrogens H_K and H_L in the central pyridine ring according to the spin system JKL ⇌ JLK. No exchange takes place with the central pyridine ring proton J, the signal of which remains sharp throughout the full temperature range. At 100 °C the dynamic process is fast on the ^{1}H NMR shift time-scale and a simplified spectrum is obtained resulting from the five averaged chemical shifts plus the shift due to H_J. It is noteworthy that at this limiting high temperature the signal J no longer exhibits a 1:2:1 triplet splitting due to coupling to H_K and H_L because the averaged shift δ_{KL} differs from δ_J by only 6 Hz at 250 MHz and thus this sub-spectrum is a strongly coupled AB_2 system with $\nu_A - \nu_B$ = 6 Hz. The observed multiplet pattern for the J, K, L hydrogens was closely simulated using a version of the LAOCOON program.[23] The result was further confirmed by predicting the spectral pattern expected at 400 MHz and comparing it with a spectrum recorded at this frequency on the SERC service instrument at the University of Warwick. Very close agreement was achieved.

The spectral changes described above closely point to a fluxional process which involves the co-ordination complex oscillating between two equivalent forms as a result of a switching of Pt–N bonding between the three N donors. The dynamics of this process was probed by applying standard band-shape analysis methods to the exchanging pairs of signals A/E, B/F and C/G, allowance being made for scalar couplings between H_A, H_B and H_C in one ring and between H_E, H_F and H_G in the other ring. Couplings involving H_D and H_H were not included so that the simulated signals for the nuclei H_C and H_G do not exactly match the experimental ones. Comparison of experimental and computer synthesised spectra are shown in Fig. 2. The calculated activation energies (see later) were based on fittings of nine experimental spectra in the temperature range −10 to 70 °C where the accuracy was greatest.

Table 2 Proton NMR data * for the aromatic protons of $[PtIMe_3(terpy)]$ in $CDCl_2CDCl_2$ at −20 and 100 °C

T/°C	δ_A	δ_B	δ_C	δ_D	δ_E	δ_F	δ_G	δ_H	δ_J	δ_K	δ_L
20	9.11	7.75	8.22	8.34	8.82	7.56	7.98	8.65	8.26	8.33	8.03
	[5.5]	[7.0]	[7.4]	[7.4]	[5.0]	[7.5]	[7.5]		[8.0]	[8.0]	[8.0]
	[1.5]	[5.5]	[7.0]		[1.5]	[5.0]	[7.5]		[8.0]		
		δ_{AE}	δ_{BF}		δ_{CG}		δ_{DH}		δ_J	δ_{KL}	
100		8.93	7.54		7.99		8.40		8.10	8.07	
		[≈4.5]	[7.0]		[8.0]		[≈8]		[8.2]	[8.2]	
			[4.6]		[1.6]						

* Chemical shifts relative to internal $SiMe_4$ $\delta = 0$. Scalar coupling constants (^3J/Hz and ^4J/Hz values) shown in square brackets.

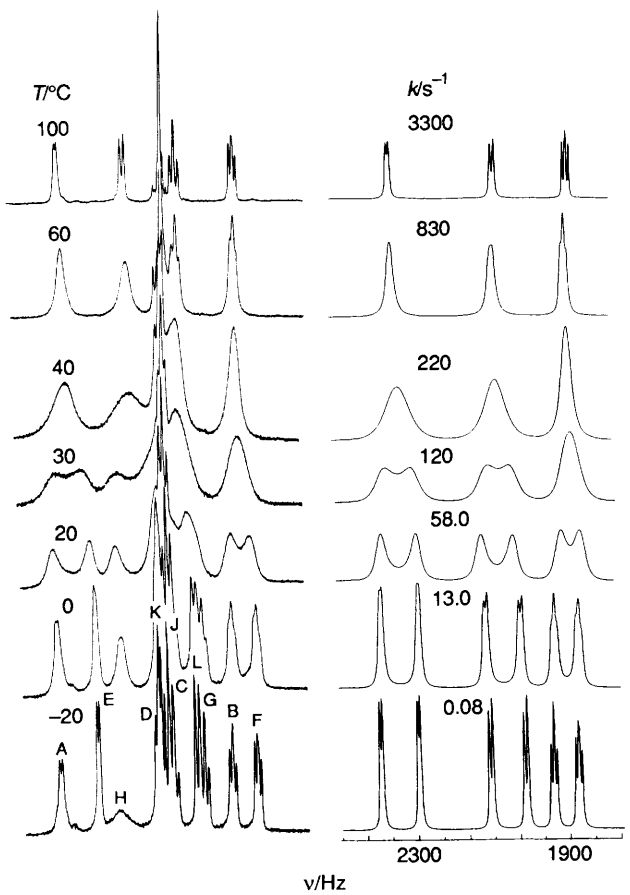

Fig. 2 250 MHz ^1H NMR spectra (aromatic region) of $[PtIMe_3(terpy)]$ in $CDCl_2CDCl_2$ in the temperature range −20 to 100 °C. Computer simulated spectra are shown on the right with 'best-fit' rate constants for the fluxional process given

Very analogous spectral changes were observed for the other complexes $[PtXMe_3(terpy)]$ (X = Cl or Br) but were not analysed in detail as the Pt–Me regions of their spectra were more informative and more accessible to analysis.

The metal–ligand fluxion referred to above manifests itself also in the Pt–Me signals of the ^1H NMR spectra. The spectra of $[PtIMe_3(terpy)]$ are again illustrative of the effect [Fig. 3(*a*) and (*b*)]. At 0 °C three sharp signals arise from the three non-equivalent Pt–Me groups. These are labelled A, B for the two equatorial environments (*i.e. trans* N) and C for the axial environment (*i.e. trans* X) (Fig. 1). Assignments were based on the observation that for the complex $[PtMe_2\{trans\text{-}(PR_3)_2\}(bipy)]^{2+}$ (bipy = 2,2′-bipyridine) the equatorial Pt–Me (*trans*-N) signal occurred at δ 1.31,[24] and that in general for *fac*-$[PtXMe_3(L\text{–}L)]$ (L–L = sulfur chelate ligands) complexes axial Pt–Me groups resonate at lower frequencies to equatorial Pt–Me groups.[25] The axial signal in the present complexes was distinctive in that it was unaffected by the metal–ligand fluxion up to *ca.* 80 °C, in stark contrast to the equatorial Pt–Me signals. The equatorial Pt–Me_B adjacent to the unco-ordinated pyridine ring appears at an abnormally low frequency due to the strong shielding effect of this aromatic ring (see later).

All three Pt–Me signals have associated ^{195}Pt satellites and their $^2J(PtH)$ values can be related to the *trans* influences of the co-ordinated nitrogens.[26] It will be seen from Table 3 that for all three complexes $^2J(PtH)$ magnitudes are greater for Me_A than Me_B methyls, implying that N^1 exerts a weaker *trans* influence than N^2, and hence that N^1–Pt bonds are slightly stronger and shorter than N^2–Pt bonds. This conclusion is compatible with the X-ray crystal data of $[PtIMe_3(terpy)]$ (see later).

On warming $CDCl_2CDCl_2$ solutions of all three complexes, the two equatorial Pt–Me signals exhibit gross broadening which lead to coalescence at *ca.* 50 °C followed by sharpening to an exchange-averaged signal at *ca.* 90 °C. Platinum-195 satellites are also just visible at this temperature [Fig. 3(*b*)]. The axial Pt–Me signal is essentially unaffected during this temperature variation, but at *ca.* 90 °C for complex **3** it is just starting to broaden. This effect gathers momentum on further elevation of temperature, when there is noticeable exchange occurring between axial and equatorial Pt–Me signals. Such an exchange or scrambling of Pt–Me environments is a well known feature of *fac*-$[PtXMe_3(L\text{–}L)]$ compounds.[27]

Band-shape analysis was applied to the Pt–Me regions of the ^1H spectra of all three complexes. At temperatures from 0 to 40 °C (70 °C for X = Cl) spectra were sensitive to a single rate constant k_{AB} for exchange between the two equatorial Pt–Me groups. At higher temperatures, the spectral band shapes became sensitive also to a rate constant, k_{AC} or k_{BC} representing axial–equatorial exchanges. The 'best-fit' values for the X = I complex **3** are given in Fig. 3(*a*) and (*b*).

Energies of the Pt–terpy *and* Pt–Me *Fluxions.*—Activation parameters for these two fluxional processes were calculated from 'best-fit' rate data and are collected in Tables 4 and 5. For complex **3** values for the Pt–ligand fluxion were based on changes in both the aromatic and Pt–Me regions. The $\Delta G^{\ddagger}$ (298.15 K) parameters are quoted with statistical errors (E_S) based on the scattering of k values around the Eyring straight line only, with errors due to systematic errors in rate constant and temperature measurements (E_{kT}) based on the equation $(\sigma_{\Delta G^{\ddagger}}/\Delta G^{\ddagger})^2 = [1 + (\ln \alpha)^{-1}]^2(\sigma_T/T)^2 + [\ln \alpha]^{-2}(\sigma_k/k)^2$ ($\alpha = k_B/h)(T/k)$,[28] and with total errors (E_{tot}).

Values of $\Delta G^{\ddagger}$ for the metal–ligand commutation are in the narrow range 61.5–62.5 kJ mol^{-1} and exhibit no halogen dependence. On account of the novelty of this fluxion no corresponding values are available for comparison purposes. $\Delta G^{\ddagger}$ Values for the Pt–Me scrambling fluxion are in the range 73.9–84.1 kJ mol^{-1}, and do show a slight halogen dependence such that Cl > Br > I. These values are somewhat lower than those associated with the analogous fluxion in platinum(IV) complexes with co-ordinated chalcogen chelate ligands where magnitudes in the range 83–90 kJ mol^{-1} are more usual[27] and halogen dependency is not observed.

Table 3 Proton NMR data[a] of the Pt–Me signals of [PtXMe$_3$(terpy)] (X = Cl, Br or I) in solution at different temperatures

X	T/°C	δ(Me$_A$)	^2J(PtH)	δ(Me$_B$)	^2J(PtH)	δ(Me$_C$)	^2J(PtH)
Cl	−90[b]	1.24	73.0	−0.02	69.4	−0.08	73.6
		1.20[d]	?	0.06[d]	?	0.91[d]	≈73
	−10[b]	1.33	74.2	0.11	69.8	0.12	≈70
	100[c]	0.88[e]	≈72			0.28	≈73
Br	−90[b]	1.33	74.0	0.02	69.7	0.06	73.8
		1.27[d]	≈70	0.15[d]	?	1.00[d]	?
	−10[b]	1.42	74.3	0.16	70.2	0.26	73.5
	100[c]	0.95[e]	≈68			0.39	≈70
I	−80[b]	1.50	74.4	0.12	70.4	0.25	72.0
		1.43[d]	72.0	0.21[d]	70.2	1.09[d]	73.0
	0[b]	1.58	75.0	0.28	70.6	0.45	72.0
	90[c]	1.06[e]	≈70			0.54	≈70

[a] Chemical shifts relative to internal $SiMe_4$ (δ = 0). Scalar couplings in Hz. [b] In CD_2Cl_2. [c] In $CDCl_2CDCl_2$. [d] Minor rotamer signals, A′, B′ or C′ identified by nuclear Overhäuser effect (NOE) spectroscopy (Fig. 5). [e] Averaged Me_A/Me_B shifts.

Table 4 Activation parameters for Pt–N fluxion in [PtXMe$_3$(terpy)] complexes

X	Temperature range/°C	$\Delta H^{\ddagger} \pm E_S$[a]/kJ mol^{-1}	$\Delta S^{\ddagger} \pm E_S$[a]/J K^{-1} mol^{-1}	$\Delta G^{\ddagger}$[b] $\pm E_S$[a],	$\pm E_{kT}$[c],	$\pm E_{tot}$[d]/kJ mol^{-1}
Cl	0–120[e]	57.90 ± 1.41	−13.7 ± 4.3	61.97 ± 0.12,	±0.66,	±0.67
Br	10–120[e]	52.90 ± 0.99	−28.8 ± 3.0	61.48 ± 0.10,	±0.66,	±0.67
I	0–120[e]	58.10 ± 2.26	−14.8 ± 6.9	62.53 ± 0.20,	±0.66,	±0.69
I	−10 to 70[f]	48.23 ± 1.60	−46.1 ± 5.3	61.93 ± 0.01,	±0.66,	±0.66

[a] Statistical errors based on k values only. [b] At 298.15 K. [c] Systematic errors in k and T values $(\sigma_k/k)_{max} = 0.2$, $(\sigma_T/T)_{max} = 6.7 \times 10^{-3}$. [d] Total errors, $E_{tot} = (E_S^2 + E_{kT}^2)^{\frac{1}{2}}$. [e] Pt–Me region signals. [f] Pyridine-ring proton signals.

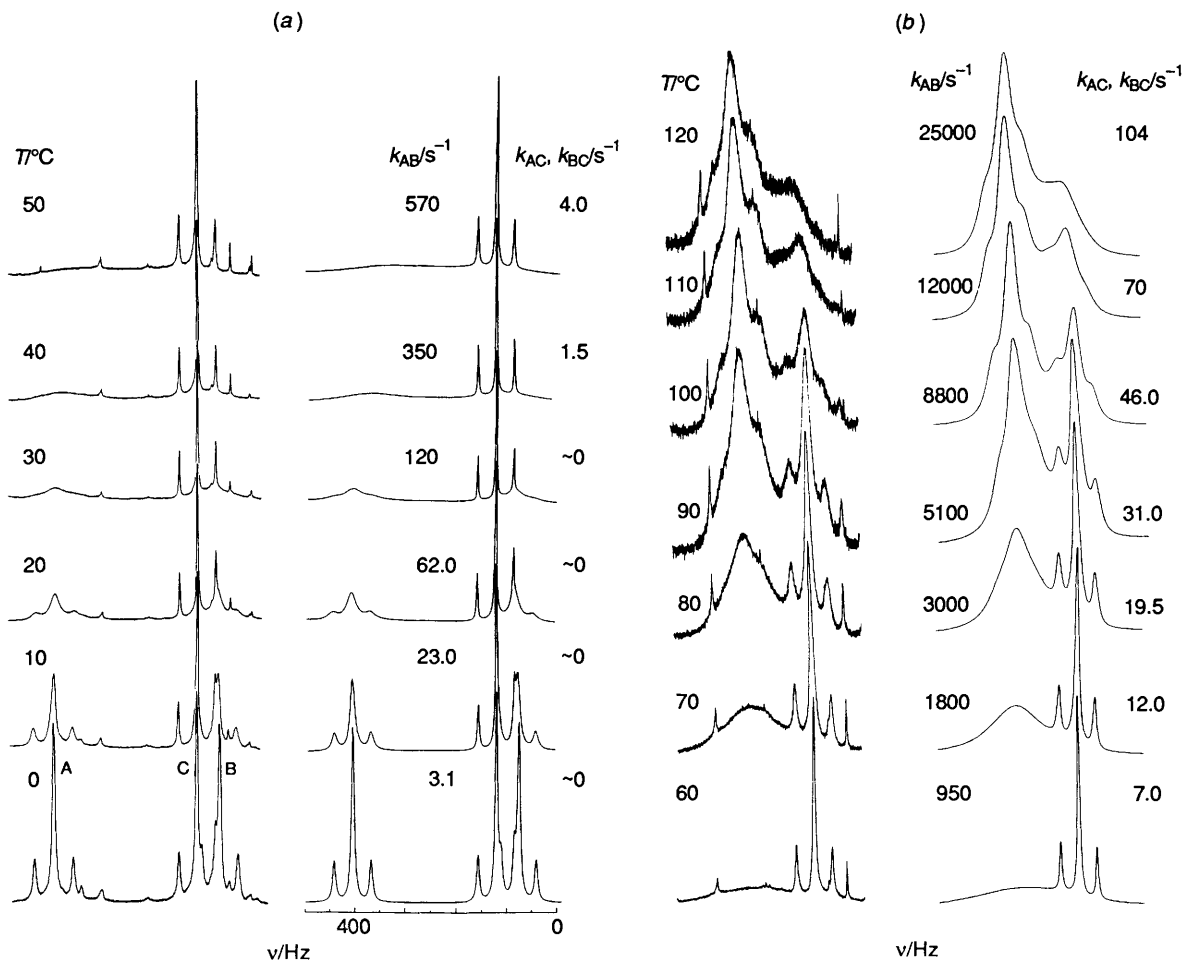

Fig. 3 250 MHz ^{1}H NMR spectra (Pt–Me region) of [PtIMe$_3$(terpy)] in $CDCl_2CDCl_2$ in the temperature range (*a*) 0–50, (*b*) 60–120 °C showing the effects of the Pt–N fluxion and Pt–Me scrambling. Theoretical spectra are shown alongside with 'best-fit' rate constants for both processes

Table 5 Activation parameters for Pt–Me fluxion in [$PtXMe_3$(terpy)] complexes

X	Temperature range/°C	$\Delta H^{\ddagger} \pm E_S{}^a$/kJ mol^{-1}	$\Delta S^{\ddagger} \pm E_S{}^a$/J K^{-1} mol^{-1}	$\Delta G^{\ddagger b} \pm E_S{}^a$,	$\pm E_{kT}{}^c$,	$\pm E_{tot}{}^d$/kJ mol^{-1}
Cl	70–120	87.39 ± 3.52	11.2 ± 9.6	84.05 ± 0.66,	±0.76	±0.98
Br	30–120	51.49 ± 0.75	−80.3 ± 2.2	75.43 ± 0.10,	±0.72	±0.73
I	40–120	49.09 ± 1.64	−83.1 ± 4.7	73.87 ± 0.24,	±0.71	±0.75

Footnotes *a*–*d* as in Table 4.

Table 6 Activation parameters for restricted pyridine ring rotation in [$PtXMe_3$(terpy)] complexes

X	Rotamer population	Temperature range/°C	$\Delta H^{\ddagger} \pm E_S{}^a$/kJ mol^{-1}	$\Delta S^{\ddagger} \pm E_S{}^a$/J K^{-1} mol^{-1}	$\Delta G^{\ddagger b} \pm E_E{}^a$	$\pm E_{kT}{}^c$	$\pm E_{tot}{}^d$/kJ mol^{-1}
Cl	0.955[e] 0.045[e]	−90 to −10	47.78 ± 1.42	−4.9 ± 6.5	49.23 ± 0.52,	±0.60,	±0.79
Br	0.924[e] 0.076	−90 to −10	45.28 ± 0.51	−15.7 ± 2.3	49.96 ± 0.19,	±0.61,	±0.64
I	0.867[e] 0.133	−90 to −10	46.55 ± 0.88	−6.4 ± 4.0	48.45 ± 0.32,	±0.60,	±0.68

Footnotes *a*–*d* as in Table 4. [e] Energy parameters are for major ⟶ minor rotamer exchanges.

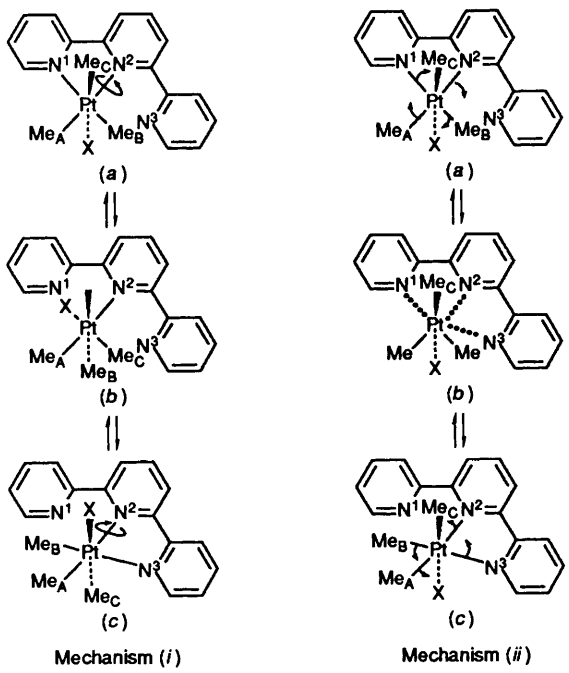

Fig. 4 Two possible mechanisms for the Pt–N linkage fluxion, namely the rotation mechanism (*i*) and 'tick-tock' twist mechanism (*ii*)

Two possible mechanisms for the Pt–N commutation may be envisaged. These are shown in Fig. 4. Mechanism (*i*) involves a loosening of the Pt–N^1 bond followed by a 180° rotation of the $PtXMe_3$ moiety about the Pt–N^2 bond to produce the original structure (*a*). This mechanism would involve a five-co-ordinate platinum(IV) intermediate. An alternative mechanism (*ii*) involves a loosening of both Pt–N bonds followed by a twist of the $PtXMe_3$ moiety through an angle equal to the N^1–Pt–N^2 angle. It involves a seven-co-ordinate intermediate or transition-state structure in which all three N donors are involved in the bonding, structure (*b*). The resulting structure (*c*) for this mechanism is the enantiomer of starting structure (*a*). In the present complexes it is possible to decide conclusively between these two mechanisms by their effects on the equatorial Pt–Me environments. Mechanism (*i*) would produce *no exchange* of equatorial platinum–methyls Me_A and Me_B, whereas mechanism (*ii*) would produce such an exchange. The NMR spectra [*e.g.* Fig. 3(*a*) and (*b*)] dramatically show such an exchange and thus it follows that in these [$PtXMe_3$(terpy)] complexes the $PtXMe_3$ moiety exhibits a novel oscillatory twist or 'tick-tock' mechanism as a result of the ligand trying but failing to adopt its more usual terdentate bonding.[1]

Mechanism (*i*) would be more likely if the Pt–N^1 bond was substantially weaker than Pt–N^2 but NMR and X-ray structural data (see later) suggest that in these complexes Pt–N^1 is somewhat stronger than Pt–N^2. In related complexes where the metal–N^2 bond is stronger the rotation mechanism may well operate. For instance, in some recent related work on complexes [$ReX(CO)_3$(L–L)] [L–L = 2,6-bis(methylthiomethyl)pyridine; X = Cl, Br or I][29] an analogous bidentate N/S fluxion occurs. Here the rotation mechanism (*i*) may be operating on account of the different Re–N and Re–S bond strengths.

Low-temperature NMR Studies.—In the ^{1}H spectra of the complexes at *ca.* −10 °C where the 'tick-tock' fluxion is slow on the NMR time-scale it was observed that the H_H and Pt–Me_C signals were significantly broader than normal. Low-temperature studies were therefore carried out on CD_2Cl_2 solutions of the complexes. Fascinating spectral changes were revealed that were clearly associated with the restricted rotation of the uncoordinated pyridine ring. The changes in the aromatic region were complex and not easy to analyse and so attention was given to the Pt–Me region. The spectra of [$PtIMe_3$(terpy)] in the range −10 to −80 °C are shown in Fig. 5. Careful observation of these changes shows that the signal C (due to Me_C) broadens dramatically on cooling reaching a maximum breadth at *ca.* −40 °C and then splitting into two very unequal intensity and widely spaced signals C and C′. Similarly, signals A and B eventually split into A/A′ and B/B′ but since the chemical shift differences between these pairs are very small little exchange broadening is observed. The limiting low-temperature spectra are clearly associated with two distinct rotameric forms of the complexes. The rotamers are such that they have very different shielding influences on the axial Pt–Me_C. This implies that the two preferred rotamers are those where the plane of the pendant pyridine ring is considerably rotated relative to the planes of the two co-ordinated rings and the heterocyclic N atom is either *cis* or *trans* to the halogen X. The large high-frequency shift of the axial-methyl ($Me_{C'}$) suggests strong deshielding by the N atom of the pendant pyridine. This implies that the major rotamer corresponds to the pyridine N atom *cis* to the halogen and the minor rotamer having N *trans* to halogen (*i.e. cis* to Me_C).

Total band-shape analysis was carried out on the Pt–Me regions of the variable-temperature spectra of the three complexes. The case of [$PtIMe_3$(terpy)] is illustrated in Fig. 5. The high quality fits led to reliable estimates of the pyridine-ring

Fig. 5 250 MHz ^{1}H NMR spectra (Pt–Me region) of [PtIMe$_3$(terpy)] in CD_2Cl_2 at low temperatures showing the effects of arresting the rotation of the pendant pyridine ring. Computer simulated spectra are shown alongside. At −80 °C, the signals A, B, C refer to the major rotamer and A′, B′, C′ to the minor rotamer

rotation energy barrier (Table 6). Values of $\Delta G^{\ddagger}$ are in the narrow range 48.5–50.0 kJ mol^{-1} and surprisingly show no halogen dependence. The nature of the halogen, however, does influence the rotamer populations with an increase in halogen mass/size slightly favouring the minor rotamer with N *trans* to halogen. Evidence of restricted rotation of pendant rings in bidentate complexes of a potentially tridentate ligand has been noted recently [2] in the case of 6-(2-thienyl)-2,2′-bipyridine (HL). In complexes such as [Rh(HL)$_2$Cl$_2$][PF$_6$] and [Ru(HL)$_2$Cl][PF$_6$], evidence of restricted rotation of the free thienyl group

Table 7 Fractional atomic coordinates ($\times 10^4$) for $[PtIMe_3(terpy)]\cdot CH_2Cl_2$

Atom	*x*	*y*	*z*
Pt	295.5(3)	1968.0(2)	2515.4(2)
I	2676(1)	1571(1)	584(1)
C(1)	1496(9)	1480(9)	3777(7)
C(2)	10(11)	30(7)	2670(8)
C(3)	−1516(10)	2202(8)	3911(8)
N(1)	−1108(7)	2568(6)	1294(5)
C(4)	−1664(10)	1765(8)	727(8)
C(5)	−2583(11)	2194(9)	17(8)
C(6)	−2983(11)	3505(10)	−139(8)
C(7)	−2401(9)	4349(8)	399(7)
C(8)	−1458(8)	3856(7)	1145(6)
C(9)	−806(7)	4705(6)	1745(6)
C(10)	−1307(9)	5988(7)	1832(8)
C(11)	−702(10)	6748(8)	2450(9)
C(12)	421(9)	6213(8)	2953(8)
C(13)	920(7)	4936(7)	2842(6)
N(2)	303(6)	4144(5)	2302(5)
C(14)	2221(8)	4420(7)	3316(7)
N(3)	3441(8)	3836(8)	2570(7)
C(15)	4638(10)	3384(9)	3067(8)
C(16)	4570(10)	3567(10)	4221(8)
C(17)	3306(11)	4203(11)	4862(8)
C(18)	2148(8)	4648(8)	4431(7)
Solvent molecule			
C(19)	4695(15)	8912(13)	2524(11)
Cl(1)	4386(5)	7331(4)	2781(3)
Cl(2)	5709(5)	9423(4)	3416(5)

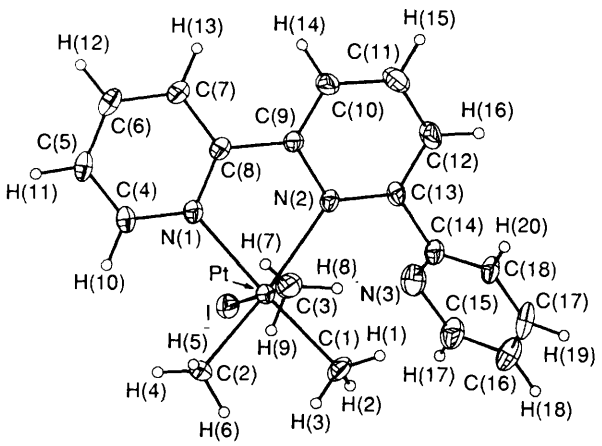

Fig. 6 A view of the X-ray crystal structure of $[PtIMe_3(terpy)]$ showing the atom labelling

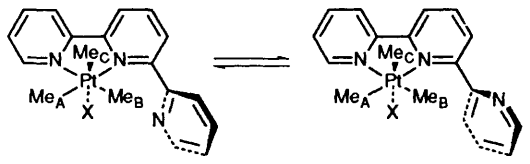

Fig. 7 Proposed solution rotamers of the complexes $[PtXMe_3(terpy)]$

was obtained but individual solution rotamers were not identified, and no energy parameters calculated.

Platinum-195 *NMR Spectrum*.—An attempt was made to identify the two solution rotamers of $[PtIMe_3(terpy)]$ from its ^{195}Pt NMR spectrum as the Pt^{IV} environments should be sensitive to the orientation of the pendant pyridine ring. A single ^{195}Pt signal was detected at a shift of δ 1861.0 relative to Ξ (^{195}Pt) = 21.4 MHz. The breadth of the signal (half-height width = 75 Hz) was attributed to nitrogen quadrupole broadening. No weak signal for the minor rotamer was detected. It is just possible that the broad signal was a dynamic

Table 8 Bond lengths (Å) for $[PtIMe_3(terpy)]\cdot CH_2Cl_2$

I–Pt	2.798(4)	C(1)–Pt	2.055(10)
C(2)–Pt	2.039(9)	C(3)–Pt	2.066(10)
N(1)–Pt	2.169(8)	N(2)–Pt	2.244(8)
C(4)–N(1)	1.339(11)	C(8)–N(1)	1.344(10)
C(5)–C(4)	1.348(14)	C(6)–C(5)	1.376(13)
C(7)–C(6)	1.362(13)	C(8)–C(7)	1.409(12)
C(9)–C(8)	1.453(11)	C(10)–C(9)	1.369(11)
N(2)–C(9)	1.401(10)	C(11)–C(10)	1.376(13)
C(12)–C(11)	1.368(14)	C(13)–C(12)	1.367(11)
N(2)–C(13)	1.345(9)	C(14)–C(13)	1.487(11)
N(3)–C(14)	1.388(11)	C(18)–C(14)	1.334(11)
C(15)–N(3)	1.402(13)	C(16)–C(15)	1.368(13)
C(17)–C(16)	1.385(14)	C(18)–C(17)	1.326(13)
Solvent molecule			
Cl(1)–C(19)	1.678(16)	Cl(2)–C(19)	1.730(15)

Table 9 Bond angles (°) for $[PtIMe_3(terpy)]\cdot CH_2Cl_2$

C(1)–Pt–I	95.3(3)	C(2)–Pt–I	89.0(4)
C(2)–Pt–C(1)	85.1(5)	C(3)–Pt–I	177.3(3)
C(3)–Pt–C(1)	86.4(5)	C(3)–Pt–C(2)	88.9(5)
N(1)–Pt–I	89.2(3)	N(1)–Pt–C(1)	175.2(3)
N(1)–Pt–C(2)	96.7(4)	N(1)–Pt–C(3)	89.2(4)
N(2)–Pt–I	94.7(2)	N(2)–Pt–C(1)	101.3(4)
N(2)–Pt–C(2)	172.3(3)	N(2)–Pt–C(3)	87.2(4)
N(2)–Pt–N(1)	76.6(3)	C(4)–N(1)–Pt	125.4(6)
C(8)–N(1)–Pt	115.3(6)	C(8)–N(1)–C(4)	119.2(8)
C(5)–C(4)–N(1)	122.7(9)	C(6)–C(5)–C(4)	119.5(9)
C(7)–C(6)–C(5)	119.1(9)	C(8)–C(7)–C(6)	119.3(9)
C(7)–C(8)–N(1)	120.1(8)	C(9)–C(8)–N(1)	118.0(7)
C(9)–C(8)–C(7)	121.9(8)	C(10)–C(9)–C(8)	121.8(8)
N(2)–C(9)–C(8)	117.4(7)	N(2)–C(9)–C(10)	120.6(7)
C(11)–C(10)–C(9)	120.2(9)	C(12)–C(11)–C(10)	119.1(9)
C(13)–C(12)–C(11)	119.9(9)	N(2)–C(13)–C(12)	122.7(8)
C(14)–C(13)–C(12)	118.2(7)	C(14)–C(13)–N(2)	119.1(7)
C(9)–N(2)–Pt	110.4(5)	C(13)–N(2)–Pt	130.2(5)
C(13)–N(2)–C(9)	117.3(7)	N(3)–C(14)–C(13)	119.2(8)
C(18)–C(14)–C(13)	115.7(7)	C(18)–C(14)–N(3)	124.9(9)
C(15)–N(3)–C(14)	116.4(9)	C(16)–C(15)–N(3)	119.7(9)
C(17)–C(16)–C(15)	118.3(10)	C(18)–C(17)–C(16)	124.2(9)
C(17)–C(18)–C(14)	116.4(8)	Cl(2)–C(19)–Cl(1)	114.3(9)

average of the two rotamer signals but no variable-temperature study was conducted to examine this.

X-Ray Crystal Structure of $[PtIMe_3(terpy)]$.—This was carried out to lend support to the NMR-based arguments of the solution structures of these complexes. Atomic parameters are given in Table 7. A perspective view of the structure with its atom numbering is given in Fig. 6. Bond lengths and bond angles are listed in Tables 8 and 9 respectively.

The structure confirms both the bidentate binding of the terpyridine ligand to Pt^{IV} and the facial arrangement of the methyl groups around the metal. It shows that the terpy ligand has been forced into a non-planar arrangement of its rings with an angle of 11.92° between the planes of the two co-ordinated pyridine rings. Of greater note, however, is the fact that the structure supports the NMR prediction that the pendant pyridine ring is grossly out of plane with respect to the other two rings, and its heterocyclic nitrogen is *cis* to halogen.

The Pt–C and Pt–I distances are within the range of expected values for platinum(IV) complexes.[30] The Pt–N distances are notable in that Pt–N(2) is greater than Pt–N(1) by 0.075 Å implying a greater strength of the Pt–N(1) bond compared to Pt–N(2). Hence, by *trans* influence arguments, the Pt–C(1) bond will be longer than Pt–C(2) as is indeed the case, and this is reflected in the NMR scalar couplings, $^2J(PtH)$, where the value for Me_B is less than for Me_A in all three complexes. The central pyridine ring appears to be somewhat more distorted than the

other rings since N(2)–C(9) is 1.401 Å and N(2)–C(13) is 1.345 Å compared with N(1)–C(4) (1.339 Å) and N(1)–C(8) (1.344 Å). This is also reflected in the bond angles C(4)–N(1)–Pt (125.4°) compared with C(13)–N(2)–Pt (130.2°). The ligand bite angle N(2)–Pt–N(1) is surprisingly small at 76.6°. This is equivalent to the angle of the 'tick-tock' twist of the metal moiety in the solution fluxionality.

The equatorial methyl Me_B adjacent to the pendant ring is distorted away from the ring such that the angle N(2)–Pt–C(1) is 101.3° compared to N(1)–Pt–C(2) of 96.7°. Of particular interest is the orientation of the pendant pyridine ring. The angle between the plane of the pendant pyridine ring and its adjacent co-ordinated ring has been calculated to be 52.1°. This orientation may also be expressed in terms of the torsional angles N(2)–C(13)–C(14)–N(3) or N(2)–C(13)–C(14)–C(18) where the respective values are 54.09 and −130.54°. These data confirm the NMR observations of the solution structure. If the pendant pyridine ring was not grossly rotated with respect to the other rings then its large ring-current shielding effects on the adjacent methyl Me_B would not be observed. Some approximate calculations of this effect will now be described.

Pyridine Ring Current Effects.—The magnitude of the ring current effects on the adjacent Pt–Me_B prompted some approximate calculations based on the geometry of the solid-state structure of [$PtIMe_3$(terpy)]. Assuming that the pendant pyridine ring plane is at an angle of 52° with respect to the rest of the aromatic system it was calculated that the mean perpendicular distance of the Me_B hydrogens from the pendant pyridine ring plane was 2.44 Å, and the distance of this perpendicular vector from the ring centre was 1.26 Å. These parameters were then used in conjunction with the Johnson–Bovey[31] and Haigh–Mallion[32] theories to calculate the ring current effect on the Me_B hydrogens. The classical approach of Johnson and Bovey predicted a shielding of 1.8 ppm compared to a value of 0.7 ppm calculated from the quantum mechanical-based theory of Haigh and Mallion. Assuming that Pt–Me_A experiences negligible deshielding by the outer co-ordinated pyridine ring these values may be compared with the experimental chemical shift difference, $\delta(Me_A) - \delta(Me_B)$, of 1.29. A detailed comparison has been made between these two theories[33] and space does not permit further comment here except to note that it is stated[33] that the Haigh–Mallion predictions 'underestimate shielding in the shielding zone above the plane of the ring.' The experimental shift of 1.29 ppm therefore falls very much within current theoretical estimates.

In the above calculations it has been assumed that pyridine and benzene ring currents are of comparable magnitude and no allowance has been made for the lower symmetry, *i.e.* higher anisotropy, of the ring-current effect due to the electronegativity of the N atom and its lone pair. This additional anisotropy of the shielding effect of the pendant ring produced by the heterocyclic atom manifests itself vividly when the ring rotation is 'frozen' on the NMR time-scale. The limiting low-temperature NMR spectra indicate the presence of just two static rotamers. It is thought most likely that these solution species have structures similar to the solid-state structure where the angle between the pendant and adjacent co-ordinated ring planes is *ca.* 52°, the predominant solution species having the heterocyclic atom N(3) directed towards and *cis* to halogen and the less abundant form having N(3) directed away from and *trans* to halogen (Fig. 7). This agrees with the observed trend in relative rotamer populations where increase in the steric mass/size of the halogen increases the population of the rotamer with N(3) *trans* to halogen (Table 6). The axial Pt–Me_C will clearly be most sensitive to the orientation of the pendant pyridine ring since the ring nitrogen N(3) will change between a *cis* and a *trans* relationship with respect to Me_C. When N(3) is *cis* to Me_C a significant deshielding effect is to be expected. For the complex [$PtIMe_3$(terpy)], this rotamer shift difference, $\delta_{C'} - \delta_C$, is 0.84 (Table 3). The methyls Me_A and Me_B being in the equatorial plane of the complex will be less sensitive to the relative positioning of N(3) and therefore their shift differences for the two rotamers, namely $\delta_{A'} - \delta_A$ and $\delta_{B'} - \delta_B$ will be considerably smaller, *viz.* −0.07 and 0.09 respectively for the X = I complex.

Thus, the averaged ring-current effects of the rotating pyridine ring and the additional anisotropy of the effect caused by the heterocyclic N atom when the ring rotation is arrested can be rationalised in semi-quantitative terms.

The next paper in the series will examine the solid-state structure and solution stereodynamics of the isoelectronic series of complexes [$ReX(CO)_3$(terpy)].

Acknowledgements

We are most grateful to the Royal Society for a Visiting Fellowship (for V. S. D.). We thank Mr. Gary Ward for help with some of the calculations based on the X-ray crystal parameters. We also thank the SERC for use of the High-field NMR Facility at the University of Warwick.

References

1 E. C. Constable, *Adv. Inorg. Chem. Radiochem.*, 1987, **30**, 69.
2 E. C. Constable, R. P. G. Henney and D. A. Tocher, *J. Chem. Soc., Dalton Trans.*, 1991, 2335.
3 E. C. Constable, S. M. Elder, J. Healy and D. A. Tocher, *J. Chem. Soc., Dalton Trans.*, 1990, 1669.
4 M. C. Ganorkar and M. H. B. Stiddard, *J. Chem. Soc.*, 1965, 5346.
5 C. C. Addison, R. Davis and N. Logan, *J. Chem. Soc., Dalton Trans.*, 1974, 2070.
6 R. D. Chapman, R. T. Loda, J. P. Riehl and R. W. Schwartz, *Inorg. Chem.*, 1984, **23**, 1652.
7 A. J. Canty, N. Chaichit, B. M. Gatehouse, E. George and G. Hayhurst, *Inorg. Chem.*, 1981, **20**, 2414.
8 G. B. Deacon, J. M. Patrick, B. W. Skelton, N. C. Thomas and A. H. White, *Aust. J. Chem.*, 1984, **37**, 929.
9 N. C. Thomas and J. Fischer, *J. Coord. Chem.*, 1990, **21**, 119.
10 P. A. Anderson, F. R. Keene, E. Horn and E. R. T. Tiekink, *Appl. Organomet. Chem.*, 1990, **4**, 523.
11 E. W. Abel, N. J. Long, K. G. Orrell, A. G. Osborne, H. M. Pain and V. Šik, *J. Chem. Soc., Chem. Commun.*, 1992, 303.
12 D. F. Schriver, *Manipulation of Air-sensitive Compounds*, McGraw-Hill, New York, 1969.
13 J. C. Baldwin and W. C. Kaska, *Inorg. Chem.*, 1975, **14**, 2020.
14 D. E. Clegg and J. R. Hall, *J. Organomet. Chem.*, 1970, **22**, 491.
15 D. E. Clegg and J. R. Hall, *Spectrochim. Acta*, 1965, **21**, 357.
16 D. H. Goldsworthy, Ph.D. Thesis, University of Exeter, 1980.
17 D. A. Kleier and G. Binsch, DNMR3, Program 165, Quantum Chemistry Program Exchange, Indiana University, IN, 1970.
18 V. S. Dimitrov and J. A. Ladd, *J. Magn. Reson.*, 1979, **36**, 401.
19 V. S. Dimitrov, *Bulgarian Academy of Sciences, Commun. Dept. Chemistry*, 1985, **18**, 457.
20 V. Šik, Ph.D. Thesis, University of Exeter, 1979.
21 A. A. Danopoulos, M. B. Hursthouse, B. Hussain-Bates and G. Wilkinson, *J. Chem. Soc., Dalton Trans.*, 1991, 1855.
22 SHELX 76, G. M. Sheldrick, Program for Crystal Structure Determination and Refinement, University of Cambridge, 1976; DIFABS, N. P. C. Walker and D. Stuart, *Acta Crystallogr., Sect. A*, 1983, **39**, 158.
23 A. A. Bothner-By and S. M. Castellano, in *Computer Programs for Chemistry*, ed. D. F. De Tar, W. A. Benjamin, New York, 1968. vol 1.
24 H. C. Clark and L. E. Manzer, *Inorg. Chem.*, 1972, **11**, 2749.
25 K. G. Orrell, *Coord. Chem. Rev.*, 1989, **96**, 1 and refs. therein.
26 T. G. Appleton, H. C. Clark and L. E. Manzer, *Coord. Chem. Rev.*, 1973, **10**, 335.
27 E. W. Abel, S. K. Bhargava and K. G. Orrell, *Prog. Inorg. Chem.*, 1984, **32**, 1.
28 G. Binsch, in *Dynamic Nuclear Magnetic Resonance Spectroscopy*, eds. L. M. Jackman and F. A. Cotton, Academic Press, New York and London, 1975, ch. 3.
29 E. W. Abel, D. Ellis and K. G. Orrell, *J. Chem. Soc., Dalton Trans.*, 1992, 2243.
30 E. W. Abel, S. K. Bhargava, K. G. Orrell, A. W. G. Platt, V. Šik and T. S. Cameron, *J. Chem. Soc., Dalton Trans.*, 1985, 345.
31 C. E. Johnson and F. A. Bovey, *J. Chem. Phys.*, 1958, **29**, 1012.
32 C. W. Haigh and R. B. Mallion, *Org. Magn. Reson.*, 1972, **4**, 203.
33 C. W. Haigh and R. B. Mallion, *Prog. NMR Spectrosc.*, 1980, **13**, 303.

Received 16*th September* 1992; *Paper* 2/04971F